Natasha Sekhon, Jay L. Banner, Dan O. Breecker, and Darrel M. Tremaine. Using high-resolution x-ray computed tomography to test the suitability and guide the preparation of stalagmites for paleoclimate reconstruction. *Journal of Cave and Karst Studies*, v. 85, no. 1, p. 1-15. DOI:10.4311/2021ES0122

USING HIGH-RESOLUTION X-RAY COMPUTED TOMOGRAPHY TO TEST THE SUITABILITY AND GUIDE THE PREPARATION OF STALAGMITES FOR PALEOCLIMATE RECONSTRUCTION

Natasha Sekhon,[1,2,C] Jay L. Banner,[1,3] Dan O. Breecker,[1] and Darrel M. Tremaine[1,3]

Abstract

Stalagmites being prepared for paleoclimate analysis should typically be slabbed along the central growth axis. This is an important first step because it allows for the highest resolution of sampling with minimal over- or under-sampling of the growth layers. Further, stable isotope ratios and trace element concentrations along the central growth axis most closely record climate variability. Choosing how to slab to best expose the central growth axis for geochemical sampling is challenging based on external morphology alone. High-resolution X-ray computed tomography (XRCT) can provide the ability to discern the internal growth morphology of stalagmites non-destructively, inexpensively, and rapidly. These data can inform selection of optimal slabbing plane(s) and can help identify locations for preliminary U-series dating. We develop a conceptual screening model to assess rapidly the internal morphologies of uncut stalagmites. The specifics of screening the internal morphologies through XRCT scans include investigating the internal porosity of the sample, the number and size of voids and hiatuses, and the presence and absence of growth layers and growth axes. We demonstrate that XRCT scans capture the migration of center of growth in uncut stalagmites of both simple and complex internal morphologies. XRCT scanning facilitates the investigation of stalagmites with complex internal growth banding, opening up avenues to work on such samples when stalagmites with simpler internal morphologies are not available. Further, screening stalagmites for paleoclimate reconstructions using XRCT improves the sustainability of speleothem science by helping researchers select which stalagmites should be returned to caves without destructive slabbing, thereby minimizing impact on caves.

INTRODUCTION

Speleothems (i.e., stalagmites, flowstones) are important terrestrial archives of paleoclimate data. They form in caves and can be used to reconstruct paleoclimate trends over seasonal to orbital timescales (Atsawawaranunt et al., 2018; Comas-Bru et al., 2020). Paleoclimate reconstructions are typically performed by milling or ablating material from the central growth axis of a speleothem, then measuring time-resolved variations in oxygen isotope ratios (proxies for rainfall amount and for moisture source), carbon isotope ratios (proxies for vegetation type/productivity and for physio-chemical process involved in carbon transport through karst), trace-element concentrations (proxies for dissolution and for precipitation systematics in the epikarst), and growth rates (proxies for water availability) (McDermott, 2004; Lachniet, 2009; Fairchild and Treble, 2009; Wong and Breecker, 2015). Within caves, drip rates, hydrologic flow paths on cave ceilings, drip water chemistry, ventilation, geomorphology, and bedrock mineralogy can each influence the morphology of stalagmite growth layers as evidenced by numerous proxy calibration studies (e.g., Spötl et al., 2005; Banner et al., 2007; Wong et al., 2011; Tremaine et al., 2016; Czuppon et al., 2018; Carlson et al., 2020). The multitude of environmental controls makes choosing a stalagmite for paleoenvironmental reconstruction a challenging endeavor.

Stalagmites with an external morphology that promotes flat growth layers with minimal additional precipitation down the flanks (from the central growth axis) are preferred for paleoclimate reconstructions, as this architecture is thought to limit the effects of kinetic fractionation on stable isotope values ($\delta^{13}C$ and $\delta^{18}O$) (Mickler et al., 2006). Through first principles, it is also shown that stalagmite growth layers tend to pinch further away from the central growth axis (Romanov et al., 2008). Thus, stalagmite samples require slabbing close to the central growth axis such that subsequent drilling to retrieve the climate signal is not aliased through under- or over-sampling by drilling through multiple growth layers. In addition to the importance of cutting close to the central growth axis, examples of desirable internal morphology include the following characteristics: columnar calcite crystallization, limited internal porosity, and limited growth hiatuses (Frisia, 2015). Columnar calcite crystallization and its variants (open and elongated columnar calcite) suggest that minimal diagenetic alteration has occurred. Similarly, limited internal porosity suggests lower detritus contamination of calcite, and therefore, a smaller detritus-related age error.

A stalagmite with an external candlestick morphology forms when the lateral migration of the incoming drip is minimal and when the drip rate is in the correct range to promote vertical crystal extension (Baldini, 2001). These conditions

[1] Department of Geological Sciences, Jackson School of Geosciences, University of Texas at Austin, Austin, TX 78712
[2] Current address: Department of Earth and Environmental Sciences and the Institute at Brown for Environment and Society, Brown University, Providence, RI 02912
[3] Environmental Science Institute, Jackson School of Geosciences, University of Texas at Austin, Austin, TX 78712
[C] Corresponding author: natasha_sekhon@brown.edu

give rise to a singular, uniform growth axis with symmetric growth layers around the central growth axis, and they favor calcite deposition approaching oxygen- and carbon-isotope equilibrium. Here, a stalagmite containing these characteristics is also referred to as a stalagmite with simple internal growth morphologies. For this reason, candlestick-shaped stalagmites are often targeted for paleoclimate reconstruction (Dreybrodt et al., 2016; Fairchild and Baker, 2012). However, candlestick-shaped stalagmites are not always available to speleothem scientists. External morphologies that deviate from candlestick architecture, though not always ideal, can also provide useful contextual information about depositional processes (Kaufmann and Dreybrodt, 2004; Dreybrodt and Gabrovšek, 2009; Martín-Chivelet et al., 2017). It is, therefore, important to develop tools that can rapidly, non-destructively, and inexpensively interrogate the suitability of all types of stalagmites for paleoclimate reconstruction.

Here we use high-resolution X-ray computed tomography (XRCT) scans to evaluate the internal morphology (stratigraphy) of stalagmites prior to sampling. XRCT scanning of uncut stalagmites prior to slabbing/cutting is a procedure that should be implemented routinely. Not only does it provide invaluable insight into the internal morphology of stalagmite samples, but it also does so non-destructively and rapidly. Less-than-ideal samples, such as stalagmites with complex internal morphologies or those that greatly deviate from candlestick morphology, are often the only stalagmites available to address scientific questions. For such stalagmites, XRCT scans provide invaluable data that informs both the optimal slabbing plane and drilling sites for geochemical analyses. We detail important internal morphological features and establish a framework of growth characteristics through XRCT scans to evaluate the quality, and thus, the suitability of stalagmites for paleoclimate reconstruction from a morphologic perspective.

BACKGROUND

XRCT in Speleothem Science

Initially developed in the medical sciences, XRCT is an imaging technique that allows the user to view the internal structure of an object without destructive sampling. The technique stitches together multiple X-ray images taken from different angles and at different times to produce a comprehensive, three-dimensional view (in slices) of the object. In addition to its common use in the medical sciences, it is now widely used in the field of geosciences (Ketcham and Carlson, 2001; Carlson et al., 2003; Cnudde and Boone, 2013). XRCT has been employed in speleothem studies to investigate density gradients in calcite (Walczak et al., 2015), fluid inclusions (Wortham et al., 2019), textures and diagenetic alteration of calcite crystals (Vanghi et al., 2015; Bajo et al., 2016; du Preez et al., 2018), and impacts of wildfires through varying opacity signals (Miller et al., 2020). Walczak et al. (2015) further use XRCT scans to identify drilling sites on uncut stalagmites for U-series dating. Studies that use XRCT as a preliminary filter to assess the suitability of stalagmites for multi-proxy geochemical reconstructions are, however, limited (Mickler et al., 2004; Chawchai et al., 2018). To our knowledge, XRCT scans investigating stalagmites with complex internal morphologies and growths are currently not present in the literature.

Here, we use XRCT to investigate and compare the internal morphologies of two candlestick-shaped stalagmites from Florida (designated BC5 and HRC2) and one stalagmite core with more complex internal and external morphologies from New Mexico (designated SBFC9). Specifically, we analyze the changes through time in the orientation and position of growth axes on the apex of the stalagmite, in the lateral continuity in growth layers, in the spatial distribution of voids, and in the presence or absence of hiatuses to determine the best plane for slabbing these stalagmites. We slabbed the speleothem sample from New Mexico along planes guided by XRCT scans and compare the longitudinal XRCT scans and plane light (PL) images to identify drilling sites for U-series dating. This was done by identifying growth layers that were laterally continuous, contained minimal voids, and exhibited high-opacity XRCT bands. The identified sites were drilled to gather preliminary U and Th concentrations. Similarly, the XRCT scans and PL images of the samples from Florida were investigated to reconstruct their growth axes history (variability in growth axes) through time. However, preliminarily ^{14}C ages were drilled before the application of XRCT scans. XRCT scans results subsequently helped in identifying multiple voids, hiatuses, flanking of younger growth over older growth, and variability in the position of the growth axes.

SUSTAINABILITY OF SPELEOTHEM PALEOCLIMATE RESEARCH

Speleothems have historically been extracted from caves as complete pieces using rock hammers and chisels for paleoclimate investigation. The extraction of entire stalagmites greatly reduces the aesthetics of a cave, and if the stalagmite was actively precipitating calcite, the stalagmite extraction interferes with the loci of active growth. Further, reconstructing a paleoclimate record from a stalagmite is a destructive process such that replacement of the entire stalagmite after developing a paleoclimate record is very rare. A more sustainable approach of collecting stalagmites with minimal removal of entire pieces and minimum damage to the cave aesthetics is achieved through coring stalagmites using battery powered drills (Spötl and Mattey, 2012). In addition, the core hole left behind is often plugged with cave host rock to ensure the continuity of active calcite precipitation and minimum disturbance to the loci of active growth.

A recent study proposed an additional sustainable method of coring (mini-coring) the base of stalagmites to discern speleothem growth rate frequency (Scroxton et al., 2016).

XRCT scans on the retrieved core provide a non-destructive, rapid, and cheap assessment of the internal morphologies and history of migration of growth axes of the uncut, cored stalagmites. The results from XRCT scans can test the suitability and guide the preparation of stalagmites for paleoclimate reconstructions. If the internal morphology as discerned through XRCT scans of the retrieved core is deemed too complex such that a time-continuous paleoclimate record might not be possible, the uncut cored stalagmite can be returned to the cave. Further, our results demonstrate the importance of XRCT scans in their ability to capture the center of growth through depth of stalagmites that are morphologically very diverse. Speleothem Architecture Analysis provides an approach to aid in the characterization of the internal and external morphologies of stalagmites (Martín-Chivelet et al., 2017). We use the terminology provided in Speleothem Architecture Analysis to characterize the internal morphologies and history of migration of growth axes of stalagmites.

METHODS AND MATERIALS

Stalagmite Samples

Sitting Bull Falls

Sitting Bull Falls (SBF) Cave is in the Guadalupe Mountains of southeastern New Mexico, within the Permian backreef facies (Hill, 2000). The entrance to SBF Cave is behind a 45 m waterfall, and the surrounding rock precipitates as tufa. The tufa is dated to the Quaternary (Hayes, 1964). Multiple stalactites and stalagmites were removed when the cave was vandalized during the 1930s and 1940s (Nymeyer, 1978), and it is likely that undocumented vandalism has occurred since then. In many cases, the removal of stalactite tips influenced the drip location, and therefore, the axis of vertical central growth in underlying stalagmites. Following a study of trace element concentration variability in two previously cored stalagmites (Sekhon et al., 2019), a third core was retrieved from SBF Cave. The two previously cored stalagmites grew for approximately 100–150 years before 2009 CE and are each approximately 2.5 cm in length. The aim was to drill a third core that had older growth than the two previously studied.

The entrance to SBF Cave is currently restricted and monitored by the Lincoln National Forest Service to keep the cave environment pristine. Following cave preservation guidelines set by the Forest Service, a drill-mounted core barrel with an overall length of 38 cm, diamond-embedded teeth, and an external diameter of 10.14 cm was used to extract a core (Fig. 1A–C). The custom core barrel was attached to a battery powered Milwaukee M18 Rotary Hammer tool. Water was hand-pumped through the barrel during the drilling process for lubrication, to remove fine stalagmite material from the point of cutting contact, and to cool the barrel. The retrieved core (SBFC9) was extracted approximately 20 meters from the cave entrance. It was extracted in situ from the center of the stalagmite (Fig. 1C) assuming symmetrical stalagmite growth, with a single central growth axis. The initial stalactite feeding the stalagmite was plausibly broken during the period of vandalism. The current active drip location is marked by the yellow stain in Fig. 1B. The active drip location is markedly different than when the unbroken stalactite was feeding SBFC9. Therefore, we expect a rapid, monotonous spatial migration in the growth axis at minimum 80 years prior to coring. The hole left after coring and removing SBFC9 was plugged with loose cave floor sediments. Finally, the hole was filled with quick-setting concrete (Quikrete). Our research group has also used a cored piece of cave host rock as a thin cap on the drill hole when the core drill bit has a smaller external diameter. The restoration methods described here allow the stalagmite to retain its aesthetic appeal and external morphology. Further, the stalagmite continues to precipitate calcite on the restored surface.

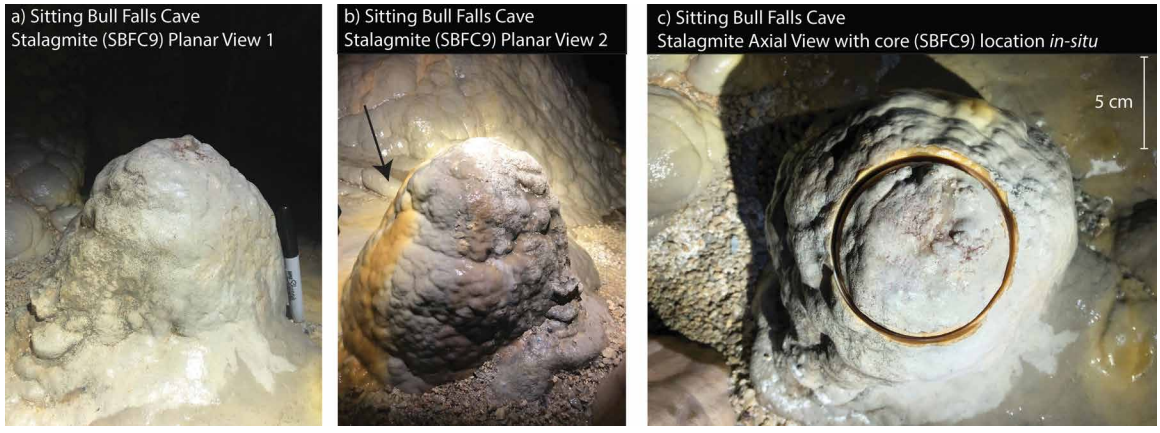

Figure 1. External views of stalagmite in situ within Sitting Bull Falls Cave. (A and B) Planar Views 1 and 2 prior to coring highlight the conical nature of the external morphology. (B) Focus of active drip location (black arrow). (C) Stalagmite axial view with core in situ. A diamond-embedded drill bit with an outer diameter of 10.14 cm was used to drill a core (SBFC9) out of this stalagmite. The circular hole in shows the drilled core prior to its extraction. The core was drilled close to the perceived central growth axis of the stalagmite.

Hollow Ridge Cave

Hollow Ridge (HR) Cave is a

well ventilated, flat-lying, phreatic-zone cave in Marianna, Florida, that formed within the Ocala, Bumpnose, and Marianna Members of the Oligocene-aged Ocala Limestone. The base passages in HR Cave are formed at the floodplain of the nearby Chipola River and are subject to flood deposition during extreme rainfall events such as atmospheric rivers and tropical storms. Regional atmospheric and cave microclimatic conditions are described in Kowalzck (2009) and Tremaine (2010).

Stalagmite sample 2 from HR Cave (HRC2) was extracted from the Smith and Jones Room, which is approximately 200 m from the cave entrance, is poorly ventilated, and exhibits maximum seasonal-temperature fluctuations of ±1 °C. HRC2 formed three meters above the cave floor atop a large slab of breakdown that hosts a cluster of stalagmites aged approximately 4000 years to the present. Farmed calcite collected under the soda straw feeding HRC2 indicates that it was actively growing at the time of collection. HRC2 is a stalagmite with a candlestick external morphology and is 28 cm in length and 5 cm in diameter at the base. It is comprised of alternating sections of fast-growing, opaque, porous calcite (averaging 75–150 μm y^{-1}) and slow-growing, clear, dense calcite that is free of voids (averaging 35–60 μm y^{-1}). After slabbing, HRC2 was subsampled at 1cm intervals for ^{14}C dating at the National Ocean Sciences Accelerator Mass Spectrometry facility. Although ^{14}C has well-understood limitations as a chronometer in speleothems, it was employed in this study because caves in Marianna, Florida, are plagued with detrital Thorium, rendering the U-Th disequilibrium dating method ineffective. Results from ^{14}C dating suggest that HRC2 grew from around 3,200 yrs BP until it was extracted in 2010 (Tremaine, 2015).

Brooks Quarry Cave

Brooks Quarry Cave (BC), located 5 km west of HR Cave, is housed within the same geologic units. A speleothem from BC, dated by U-series, suggests that the cave has been above the water table for at least 70,000 ± 5000 yrs BP (Froelich et al., 2007). BC stalagmite 5 (BC5) was extracted in 2011 during a rescue mission after the cave owner notified the Florida Geological Survey that the cave may be in danger of collapsing due to quarrying activity. BC5 is also a candlestick specimen and is 43 cm in length and 5 cm in diameter. Assuming that the candlestick shape engendered internal morphology with flat growth layers and minimal tapering toward the flanks, reconnaissance ages were obtained by sampling from the exterior using a 6mm drill bit prior to making the decision to utilize limited financial resources to continue developing BC5. Results obtained from National Ocean Sciences Accelerator Mass Spectrometry facility suggested BC5 had grown from >50,000 yrs BP through 2000 yrs BP. Also, ^{14}C dates obtained from the central growth axis after slabbing suggest that the bottom 30 cm of BC5 is older than 43,000 yrs BP and that the top 130 cm grew between 10,800 yrs BP and 2,000 a.

CT Scanning

SBFC9 was scanned at the University of Texas High-Resolution X-Ray Computed Tomography Facility using the 450-kV GE Titan X-ray source on their custom-built NorthStar Imaging, Inc. scanner. The X-ray energy was set at 300 kV and 0.85 mA, and three brass filters were used to reduce beam-hardening artifacts. The resultant CT data comprises 1,921 image slices having a voxel size/spatial resolution of 82.9 μm. The data acquisition took two hours. CT scan images were transferred as 512 × 512 8-bit JPG and 16-bit TIFF files. The adjust, orthogonal view, and transform functions in ImageJ software (Abràmoff et al., 2004) were utilized to view, process, and stack image slices. The range of 8-bit grayscale values was produced and all the scans were contrasted using ImageJ version 1.50i.

HRC2 and BC5 stalagmites were scanned at Capital Regional Medical Center in Tallahassee, Florida, using a GE Lightspeed VCT XRCT scanner. The X-ray energy was set at the machine-maximum 140 kV and 575 mA, with a spatial resolution of 600 μm per slice. A total of 481 and 721 image slices were acquired for HRC2 and BC5, respectively. The total scanning time was approximately seven hours for both specimens.

The scans allowed an in-depth 3D reconstruction of the history of migration of growth axes and internal morphology for each speleothem. Here, the vertical depth axis was set as the z axis. Further, the axial (x-y plane) and longitudinal (x-z plane) cross section views were used to investigate changes in growth history (spatial migration of growth axes or center of growth) through different vantage points. Visualization of changing growth axes in the uncut stalagmites was achieved through animating the scans using QuickTime software. Animations for the three stalagmites can be found in the supplementary files. Here, we refer to growth history moving forward with time. As such, the bottom of each stalagmite is termed as the first/earliest growth (oldest calcite precipitation in time) and the top of each stalagmite details the last/latest growth (youngest calcite precipitation in time).

RESULTS

XRCT Scan of SBFC9

Continuous to noncontinuous growth layering was observable prior to slabbing SBFC9 throughout the length of the retrieved core (Fig. 2A–E). The layers vary in thickness, coloration, and orientation of depositional surface. SBFC9's XRCT animation exhibits two major shifts in the growth phases, which correspond to three growth sections (Fig. 3A–C). The earliest growth (at the bottom) (Fig. 3C, yellow dashed circle) occurs at an approximate depth of 12 cm

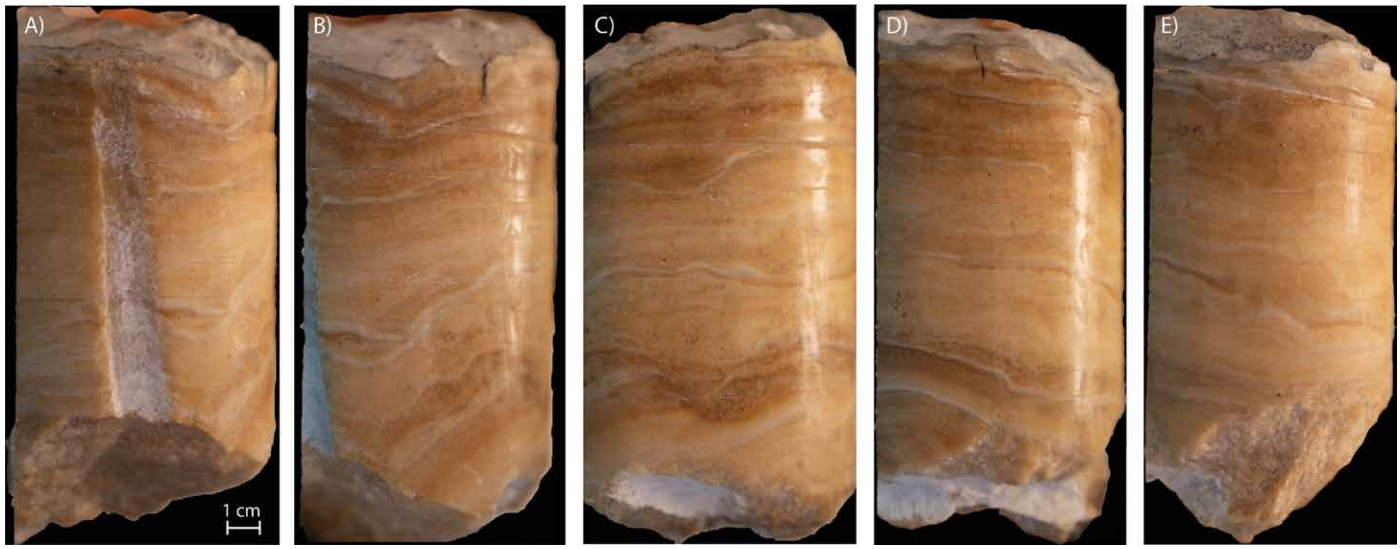

Figure 2. (A–E) Sequential views showing the clockwise rotation of core SBFC9 removed from the stalagmite shown in Fig. 1. The series of images depicts a complex internal growth morphology for SBFC9. Continuous and noncontinuous laminated bands are present throughout the entire length (14 cm) of SBFC9. The laminated bands are characterized by varying thicknesses, colors, and geometries. High-resolution XRCT scanning of this sample (Fig. 3) allows rapid, inexpensive, and non-destructive imaging to reveal the internal growth morphologies and growth history.

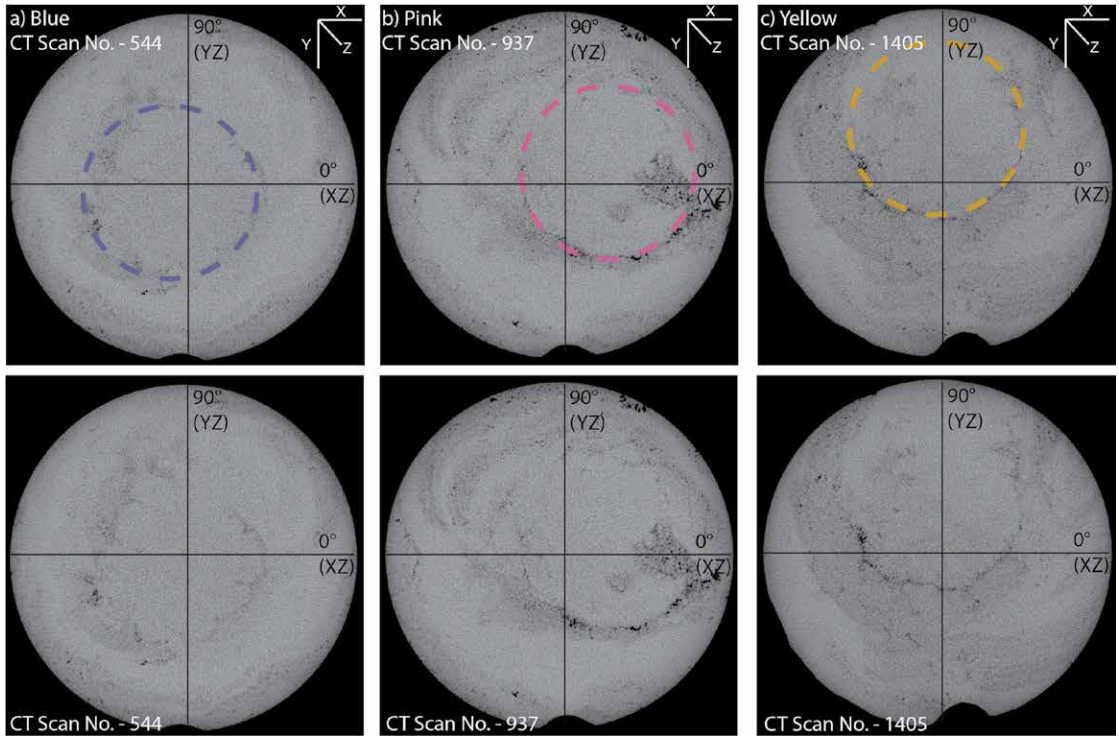

Figure 3. Three pairs of XRCT scan images of SBFC9, from sections near the top (image 544, A), middle (image 937, B), and bottom (image 1405, C). The image numbers relate to the depth from the top of the stalagmite core. The resolution through depth of each image is 82.9 µm; see Table 1 for more details regarding the relationship between scan image number and the depth from the top of the stalagmite. In the upper image of each pair, colored dashed circles are drawn based on the dominant ring of voids, which is more clearly visible in the otherwise-identical lower image of the pair. The changes from the top (dashed blue circle) to the middle (dashed pink circle) to the bottom (dashed yellow circle) highlight the spatial movement of the growth through depth. The horizontal, vertical, and depth axes (lines X, Y, and Z, respectively) define planes at 0° (black line XZ) and 90° (black line YZ) that are examples of typical cuts made on stalagmites in the absence of XRCT scan imagery.

(Table 1). To note, approximately 3 cm of the core broke during the core removal procedure (Fig. 2). This growth is labeled Remaining Growth in Table 1. The remaining growth is not discussed further. After growing for approximately 3.87 cm, a change in the spatial orientation of growth deposition begins (Fig. 3B, pink dashed circle) at around a depth of 7.74 cm from the top of the stalagmite. The second growth section is about 3.23 cm in vertical deposition with a lateral shift of approximately 2.7 cm from the earliest growth. This leads into the third and last growth section (Fig. 3A, blue dashed circle) at a depth of approximately 4.51 cm from the top of the stalagmite. The center of the migrating growth section is the center of the circle characterized by a cluster of dark points (low contrast in the XRCT scans) that depict either void spaces or

Table 1. Major growth sections for SBFC9.

Growth Section	1	2	3	4
Color in Figs. 3–4	Blue	Pink	Yellow	Remaining Growth[a]
Relative Age	Youngest	Older	Older	Oldest
CT Scan Numbers	1–544	545–937	948–1405	1406–1921
Thickness (z axis) (cm)	4.51	3.23	3.87	4.26
Depth from top[b] (cm)	0–4.51	4.51–7.74	7.74–11.61	11.61–15.87

[a] During the removal of SBFC9 from the stalagmite, the core broke off at an angle. From Fig. 2, remaining growth covers the angular section (approximately 3 cm) toward the bottom.
[b] Depth from top is the range from the top of the growth section to the bottom of the section, measured from the top of the stalagmite.

crystallographic features (Fig. 3A–C, dashed circles). The spatially large shifts in growth deposition (Table 1) are a feature of the complex internal growth morphology of SBFC9.

As outlined above, the primary aim of slabbing a stalagmite is to cut as close to its central growth axis as possible to optimize stable isotope and trace element geochemical analyses. A simple internal growth morphology with a singular central growth axis with minimal spatial migration increases confidence in slabbing an uncut stalagmite along a central growth axis. However, a stalagmite with a relatively complex internal growth morphology, such as SBFC9, requires a more thorough investigation. The characterization of the complex internal morphology as inferred from XRCT scans was used to develop a strategy to slab stalagmite SBFC9 through the center of the colored circles (Fig. 4, black dashed lines), assuming the center of the colored circles to be the center of a growth axis.

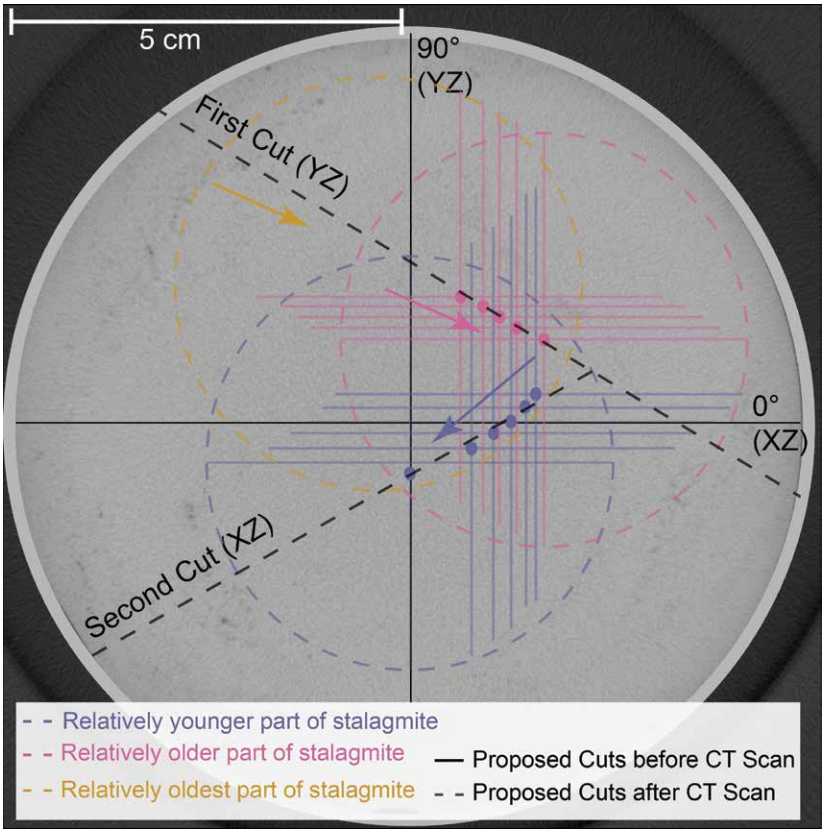

Figure 4. The complex growth history of SBFC9 recorded by XRCT scans. XRCT scans reconstruct in great detail the position and orientation of growth over time for SBFC9. Proposed cuts before XRCT scans (solid black lines) were along the 0° and 90° planes. However, the spatially shifting growth of SBFC9 through depth is discerned through careful investigation of XRCT. Updated planes for slabbing the core for usable geochemical sample transects are indicated by dashed black lines. The first cut (dashed black line YZ) is positioned to best capture the center of growth of the 2 oldest (yellow and pink) growth sections. The second cut (dashed black line XZ) is positioned to capture the center of growth of the youngest (blue) growth section. The assumed position of center of growth (blue and pink and cross hairs within their respectively colored circles) is based on scan results from different depths. Arrows indicate the migration of center of growth from older (first growth) to younger (last growth) parts of a growth section.

The proposed cuts guided by XRCT scans (Fig. 4, black dashed lines) differ substantially from the slabbing planes identified solely on the sample's external morphology, i.e., prior to analyzing the XRCT scans (Fig. 4, solid black lines). Typical slabbing planes based solely on external morphology, the x-z or y-z planes, completely miscaptured the center of the growth section, as the center of growth spatially migrated through time. The proposed first cut based on the XRCT results (Fig. 4, First Cut (YZ)), however, is aligned to cut through the center of the colored circles as growth migrates from the earlier (yellow) to older (pink) areas. The second proposed cut (Fig. 4, Second Cut (XZ)) is then aligned to cut through the center of the youngest growth (blue) area. The XRCT scans, therefore, informed the strategy followed to slab and section SBFC9. However, the cross-sectional assessment of XRCT scan, reinforced by the cross-section of the slabbed sample through PL imaging, suggests that the growth sections and the cross hairs do not reflect the center of a migrating growth axis (Fig. 4) but instead the center of growth of a rimmed micro-terrace (discussed in detail below). The spatial migration of the center growth (Fig. 4, colored arrows) visible through XRCT scans is a robust result that provides insight into the internal morphology of the uncut stalagmite core.

XRCT Scans of HRC2 and BC5

The XRCT scans of the Florida stalagmites, HRC2 (Fig. 5) and BC5 (Fig. 6), illustrate comparatively modest lateral migration of growth (about 1 cm) and, by extension, drip migration

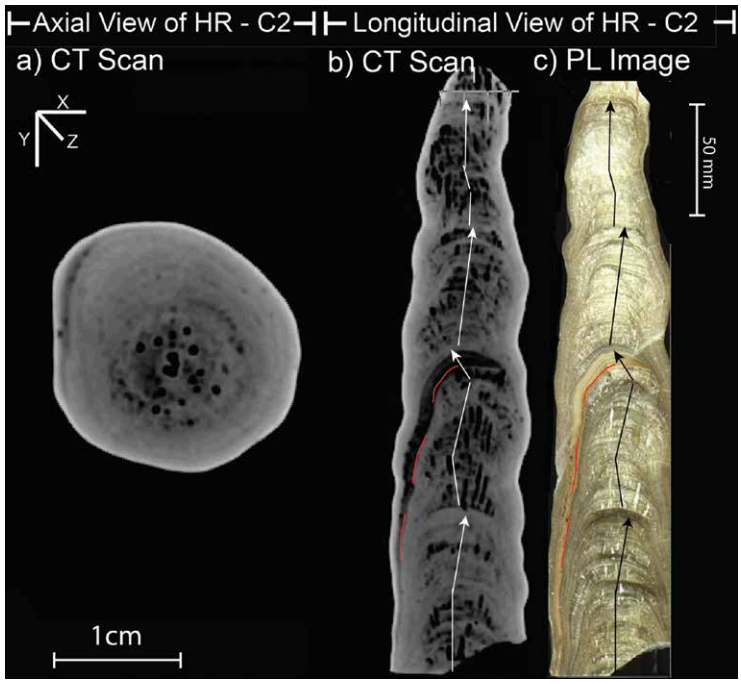

Figure 5. HRC2 from Hollow Ridge Cave. (A) XRCT scan axial view of HRC2. Clear concentric dark and light circles suggest a typical stalagmite growth structure with minimal growth migration. Lines X, Y, and Z signify horizontal, vertical, and depth planes, respectively. (B) Longitudinal XRCT scan along the XZ plane showing migration of growth axes (white arrows). (C) PL image corresponding to the XRCT scan in B.

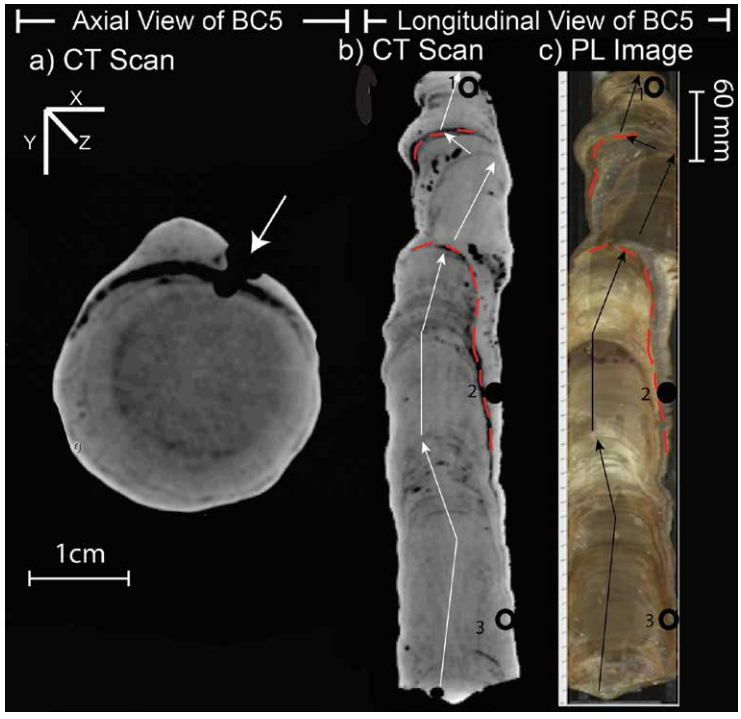

Figure 6. BC5 sample from Brooks Quarry Cave. (A) XRCT scan axial view of BC5. Clear concentric dark and light circles suggest a typical stalagmite growth structure. Lines X, Y, and Z signify horizontal, vertical, and depth planes, respectively. (B) XRCT scan longitudinal view along the XZ plane showing migration of growth axes (arrows) and locations where samples were drilled for radiocarbon dating before slabbing (black circles 1, 2, and 3). (C) PL image corresponding to the XRCT scan in B. One drill location (solid black circle 2 in B and C, and white arrow in A) is a younger date than expected.

histories. The axial view of the XRCT scan for HRC2 (Fig. 5A) exhibits concentric circles, which increased in circumference as HRC2 continued to grow. Voids (darker spaces on the XRCT scan) are noted through the entire length of HRC2 in the longitudinal plane (Fig. 5B). Minor changes in the central growth axis are also recorded by the XRCT scan of HRC2 (Fig. 5B, white arrows). PL images replicate the changes in growth axes post-slabbing (Fig. 5C, black arrows). A crystallographic anomaly in the XRCT scan is visible in plain light as an orange-colored rind (Fig. 5B–C, dashed red line).

The axial (Fig. 6A) and longitudinal (Fig. 6B) views of BC5 indicate 3 significant changes in growth axis demarcated as dark bands in the XRCT scans. Over the latest 60 mm of growth, the central growth axis of this stalagmite oscillated approximately 20 mm to the right and then approximately 30 mm to the left (Fig. 6B). The change in growth direction of the center of stalagmite deposition (Fig. 6B, white arrows) was reconstructed with XRCT imagery. Internal growth layers are visible as low and high opacity bands in the XRCT scans (Fig. 6B). Post-slabbing PL images indicate that crystallographic features associated with low opacity (darker) in the XRCT scan are visible as an orange-colored rind (Fig. 6B–C, dashed red line).

DISCUSSION

Reconstructing Deposition Processes Using XRCT Scans

Each XRCT scan was stitched together as an animation that spanned the entire length from the bottom (earliest growth) to the top (latest growth) of every stalagmite sample. The animations were then studied for multiple features: distribution of voids, consistency of growth layers characterized as contrasts in XRCT opacity, and the change in orientation and position of growth axis through depth. These three features exert a strong influence on the likelihood of producing a robust, high-fidelity paleoclimatic record using just 1 cut to slab the speleothem. The presence of voids increases the porosity of the sample, which increases the chance of sampling diagenetically altered calcite in contact with inclusion water of variable age (van Bruekelen et al., 2008), and hence may reduce the quality for paleoclimatic reconstruction. Calcite laminae density is a function of crystal morphology and affects the opacity viewed in XRCT scans. More porous columnar calcite suggests faster growth, high porosity, and abundant fluid inclusions. Conversely, dense compact calcite suggests slow growth, low porosity, and minimal fluid inclusions (Frisia, 2015; Boch et al., 2011). Calcite density has also been shown to decrease during hiatuses (Webster et al., 2007). The presence of hiatuses provides insight into changes in the depositional environment that may include

decreased drip water volumetric input, changes in cave ventilation, a rise in water table height, or migration of the drip site on the cave ceiling. As previously discussed, sampling nearest the central growth axis of an uncut stalagmite is necessary to avoid the added uncertainties imparted onto stable isotope ratios and trace element concentrations through kinetic fractionation.

The following sections discuss stalagmite-specific deposition processes in each cave. Axial and longitudinal (planar) views of the XRCT scans reveal a range of depositional processes and the history of migration of growth axes.

Hollow Ridge Cave, Florida (HRC2)

HRC2 has a relatively consistent and singular central growth axis that exhibits only a handful of minor directional variations. The internal morphology of HRC2 includes both aggradational and retractional patterns as defined in the Speleothem Architecture Analysis (Martín-Chivelet et al., 2017). Briefly, aggradational stacking patterns detail uniform vertical growth that is fed by constant and regular drips, indicative of a constant volumetric supply and a regular drip rate with a low coefficient of variation. Retractional stacking patterns detail nonuniform growth that is fed by irregular drips under a changing volume supply. Under similar hydrochemical conditions of $CaCO_3$ saturation, aggradational and retractional patterns are formed by constant and decreasing drip rates, respectively (Dreybrodt 1999; Dreybrodt et al., 2016; Munoz-Garcia et al., 2016; Martín-Chivelet et al., 2017). The transition from aggradational to retractional is noticeable in Fig. 5B–C as the diameter of the stalagmite narrows towards the later part of growth with minimum change in drip site location.

The internal morphology of HRC2 is characterized by an abundance of voids cutting vertically through growth layers (Fig. 5A–B). It is unknown whether these voids contained fluid inclusions prior to slabbing. These voids vary between 1–5 mm in vertical length in the direction of the growth axis, are approximately ellipsoidal in shape, and are present in four discrete sections throughout the vertical length of HRC2. It is possible that the voids were formed erosively, post-calcite deposition (e.g., Zisu et al., 2012). Calcite was actively farmed atop HRC2 for three years prior to removal, and dripwaters in the Smith and Jones Room were observed to be supersaturated with respect to calcite (Ω ranged from approximately 5.5 to 26.9) over a four-month period during the winter of 2009–2010 (Tremaine et al., 2011). Together, these characteristics suggest that modern dripwater is non-corrosive to speleothems, but that does not rule out the possibility that ancient drips became undersaturated and eroded the speleothem from the tip down over certain intervals.

Isotopic and trace element behavior in HRC2 suggest that the voids occur during dry or drying intervals (Tremaine, 2015). The voids are likely a result of decreased rainfall and drip rates, increased prior calcite precipitation, and a resultant drip that was slightly undersaturated with respect to calcite. XRCT scan and density analyses that investigate the migration of void spaces through depth proved useful because most void spaces were smoothed away in the slabbing and polishing process and would not have otherwise been considered in the paleoclimate reconstruction as the void spaces. Therefore, investigating the internal morphology through XRCT scans provides a first order estimation on the drip water supply.

Brooks Quarry Cave, Florida (BC5)

BC5's axial (Fig. 6A) and longitudinal (Fig. 6B) XRCT scans depict stable deposition processes for the earliest approximately 140 mm of stalagmite growth, followed by a change in drip location and subsequent growth deposition of approximately 60 mm. The next approximately 200 mm of growth roughly followed a similar change in drip location. The change in drip location is demarcated as a thin, low-density segment that cascades down the side of the stalagmite (Fig. 6B–C, dashed red line). Radiocarbon dates suggest that this low-density section is a hiatus separating the earlier-growth segment (>50,000 a) from the Holocene-aged segment beginning at 10,800 yrs BP (Tremaine, 2015). The growth axis exhibits a marked shift at the beginning of the Holocene section that persists for approximately 80 mm before another marked shift in the opposite direction. This shift in growth direction is associated with another thin low-density segment (Fig. 6B–C, dashed red line) that may indicate a hiatus. BC5 is characterized by dense calcite growth throughout as inferred by the brighter (high opacity) XRCT scans and minimal voids.

Perhaps the most important aspect of the XRCT scan of BC5 is that of dating the stalagmite. Reconnaissance ^{14}C dating of BC5 suggested ages that were suitable for further analysis (approximately 48,000 a at the bottom, 10,800 a in the middle, and 2000 a at the top of the stalagmite in Fig. 6). BC5 was then slabbed and polished. Subsamples were collected and analyzed for ^{14}C, a costly and time-consuming process. However, thorough investigation of XRCT scans later revealed that the middle pilot date (drilled from the outside) of 10,800 yrs BP (Fig. 6A, white arrow; Fig. 6B–C, 2) had been primarily collected from a thick layer of overgrowth that had precipitated down the flank on one side. This overgrowth represented calcite deposited after a hiatus and was approximately 30,000 yrs BP younger than the targeted section. Fig. 6A shows that the tip of the drill barely encountered the ancient portion of the stalagmite, indicating that 10,800 yrs BP is the date of the material precipitated after the first hiatus. A closer inspection of the XRCT scans prior to slabbing, sectioning, and subsampling for additional ^{14}C dates would have identified the dating error and paused the development of BC5, saving substantial time and money.

Like HRC2, BC5's internal growth morphology trends from aggradational in the earlier portion to retractional in the later growth sections of BC5. A probable explanation for this shift in the internal architecture is an increased rate of post-splashdown CO_2 degassing with minimal change in drip rate. As such, calcite precipitation would be faster with minimal change in drip rate, leading to a flattened top with a larger surface area of horizontally aligned growth layers. The increased rate of CO_2 degassing while maintaining other calcite precipitation controls constant could be attributed to changes in the ventilation regime or to biogeochemical variability in the soil above the epikarst. Alternatively, changes in drip rate, to saturation level of calcite, and in drip path in the epikarst might be responsible for the change from aggradational to retractional in BC5.

Sitting Bull Falls Cave, New Mexico (SBFC9)

Stalagmite SBFC9 was scanned at a much higher spatial resolution than HRC2 or BC5 (82.9 µm versus 600 µm per scan, respectively), resulting in 1,921 individual slices. SBFC9's axial and longitudinal XRCT scans (Fig. 7A–B) reveal an internal growth morphology that is more complex than that of HRC and BC stalagmites. XRCT scans of SBFC9 suggest significant change in position and orientation of its growth axes, multiple apices of calcite growth, an absence of consistent and continuous growth bands around a central drip point, and clusters of small (1 mm) voids.

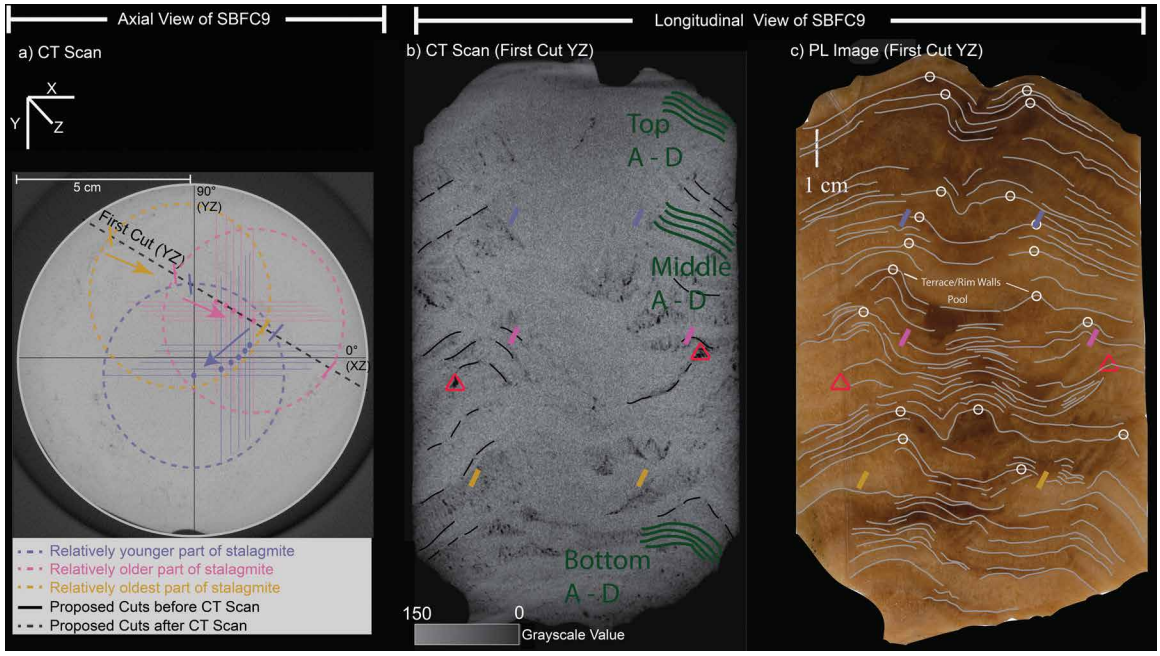

Figure 7. First cut of SBFC9 using XRCT scan information. (A) Axial view of SBFC9 with first cut (dashed black line YZ) through the 2 oldest (yellow and pink) growth sections from Figure 4. (B) XRCT longitudinal view of the first cut detailing the complex internal morphology that is absent of continuous growth bands, showing visible growth bands (black dashed lines), void spaces with an 8-bit grayscale value of 0 (red triangles), the local apex of growth over the 3 main growth sections (yellow, pink, and blue slashes), and growth bands that were sampled for preliminary the U-series analysis in Table 2 (green lines top A–D, middle A–D, and bottom A–D). (C) PL image corresponding to the XRCT scan in B and showing growth layers (gray lines) and highlighting multiple growth peaks or highpoints (white circles).

Typically, a wide distribution of voids and an absence of a central and singular growth apex that pinches out towards the flanks as revealed through XRCT scans would hinder the identification of robust drilling sites for U-series dating and subsequent geochemical (stable-isotope and trace-element) analyses. Age reversals through secondary calcite precipitation in voids could affect the precision of U-series dating. And an absence of a central and singular growth axis complicates identifying continuous milling tracks for geochemical analyses. However, careful tracking of growth sections as achieved via XRCT scans provides planes for optimal slabbing to retrieve sites for radiometric dating and geochemical analyses. The axial view of SBFC9 (Fig. 3) highlights the growth sections. The XRCT longitudinal view of SBFC9 (Fig. 7B) along proposed cuts does not reflect the clear spatial migrations of the growth sections that are visible in the axial view (animation in supplementary files). The internal growth morphology of SBFC9 follows progradational patterns that are generated by increasing drip rates (Munoz-Garcia et al., 2016). However, the absence of a central and singular growth axis through the entire length of the core further suggests multiple changes in the position of drip onto the stalagmite surface. Nonetheless, the inferred continual and spatially dramatic changes in drip rates would suggest a more conduit- or fracture-fed drip than a diffuse-fed drip.

Comparing XRCT Scans with PL Images

Following an investigation of the XRCT scans and using the reconstructed growth history (the history of the migration of growth) as a guide to slab and section, subsequent high-resolution PL imaging detailed information on central growth axis and continuity of growth layers. Concurrent use of XRCT scans and PL images on the same cut-plane can

aid in developing tracks for geochemical (stable-isotope and trace-element) and geochronological (radiocarbon and U-series) analyses. PL images for HRC2 and BC5 are generally reflective of the growth information contained in XRCT scans. XRCT scans as animations were clearly able to delineate crystal morphology and voids through depth beneath the surface. The orange-colored feature in the PL image of HRC2 is observed to be a low-density (opacity) layer in the XRCT scan. Similar features are observed in BC5. In this study, HRC2 and BC5 are characterized by simple growth.

SBFC9's PL images reveal a complicated growth history that provides complementary information to the XRCT scans. For SBFC9's cut, void spaces with an 8-bit grayscale value of 0 (Fig. 7B, red triangles) are not clearly captured through either the corresponding PL image (Fig. 7C) or through visual hand inspection. Further, animation through depth of XRCT scans suggest that the void spaces are at least 0.5 mm in depth. This is not possible to discern through two-dimensional PL images or visual inspection. PL images capture the growth bands seen in XRCT scans (Fig. 7B, dashed black lines).

Tracking growth layers in the longitudinal PL image (Fig. 7C, gray lines) elicits two possible depositional processes that were not clearly visible through XRCT scans alone. The first possible process is that SBFC9 was fed by two stalactites or soda straws, which led to the growth of two independent stalagmites. If the two stalagmites were growing next to each other, the growth layers at the local low-point would overlap and cut each other. The growth layers would further pinch out towards the flanks of the two stalagmites, which is not observed through XRCT scans or PL images. Conversely, the growth layers are continuous at the local low-points between the possible two growing stalagmites. A more likely cause of the complex internal morphology of SBFC9 is the presence of micro-terrace-like structures. Micro-terrace-like structures akin to rimstone pools and travertine terraces have been observed on stalagmite surfaces and on a much larger scale of tens of centimeters (Jettestuen et al., 2006; Dreybrodt and Gabrovšek, 2009; Shtober-Zisu et al., 2014).

Speleothem Architecture Analysis defines a rimmed stalagmite unit as a small basin (pool) surrounded (rimmed) by an upward bulge (Martín-Chivelet et al., 2017). Hammer et al. (2010) suggests that turbulent flow along the rimmed dams preferentially deposits calcite in the upward structure of micro-terraces leading to a low-lying pool of water surrounded by relatively high-calcite terraces. The longitudinal PL image of SBFC9 suggests a basin with corresponding high-points (Fig. 7C, white circles). The positions where the slab path cuts the inferred growth circles in SBFC9 are close to the apex of these localized high points (Fig. 7B–C, slash symbols). As such, the XRCT scans of SBFC9 record the center of growth for the micro-terraces similar to the macro-scale rimstone dams where the rim of the dam, due to more turbulent flow, gets more agitated, grows faster, and as a result plausibly has more voids (Hammer et al., 2007; Hammer et al., 2010). Absent exceedingly strong airflow in the back of the cave, which is unlikely to have occurred, SBFC9 being precipitated from a single soda straw can be ruled out. In conclusion, the proposed cuts for SBFC9 following XRCT scans slabbed the core along the center of growth, which is the pool surrounded by micro-terraces.

The growth layers in XRCT scans reflected by low-density bands (i.e., 8-bit grayscale values ranging between 10–70) correspond to the darkest orange-colored bands in the PL images. High density sections (8-bit grayscale values close to 150) in XRCT scans are reflected as clear white bands in PL images. A possible explanation is that the high-density sections reflect dense calcite fabrics. Conversely, the low-density growth bands either reflect porous calcite fabrics or reflect organic matter inclusions in calcite growth layers that could explain the orange-colored bands. Lastly, sampling locations for U-series dating (Fig. 7B, green lines top A–D, middle A–D, and bottom A–D) were informed following insights gained through comparing XRCT scans and PL images. Preliminary tracks were drilled along growth layers that had high-density calcite, did not have any void spaces, had continuous growth layers that were optimal drilling tracks for U-series as post-depositional diagenesis, and had considerably-reduced contamination through detrital material (Fairchild and Baker, 2012). The first two characteristics were informed through XRCT scans and PL images that helped to identify sections with continuity in growth layers. Preliminary tracks acted as testbeds to quantify the concentrations of U and Th before drilling the approximately 600 mg of calcite that is required for thermal ionization mass spectrometry U-series dating. The drilled samples were analyzed for U and Th concentrations using a quadrupole inductively-coupled plasma mass spectrometer. Adequate concentrations of U (500−600 ppb) and below detection limit concentration of Th (10 ppt, Table 2) confirm that the layers selected using XRCT scans and PL images optimize slab selection to retrieve ages through thermal ionization mass spectrometry U-series dating even in a complex-growth stalagmite. A similar approach comparing XRCT scans and PL images can be used to find the best-suited tracks for geochemical (stable-isotope-ratio, fluid-inclusion, and trace-element) analyses.

Investigating Suitability for Paleoclimate Reconstructions

As dripwater falls from the cave ceiling onto the surface of a stalagmite, it encapsulates a snapshot of multiple hydroclimate proxies. Through time, the stalagmite archives the data in its vertically growing layers. Thus, to best reconstruct paleoclimate data, it is important to determine the central growth axis and its flanks (reflecting a singular dripwater), because that is where the proxy signal is least affected by in-cave processes that enhance kinetic

Table 2. U and Th concentrations for SBFC9 at the sampling locations shown in Figure 7B.

Tracks	U (ppb)	Th (ppt)[a]
Top A	610	BDL
Top B	528	BDL
Top C	552	BDL
Top D	482	BDL
Middle A	558	BDL
Middle B	546	BDL
Middle C	500	BDL
Middle D	550	BDL
Bottom A	532	BDL
Bottom B	543	BDL
Bottom C	537	BDL
Bottom D	569	BDL

[a] BDL = below detection limit (10 ppt).

fractionation on stable-isotope values and PCP effects on trace-element ratios. Growth rates calculated via counting laminae couplets are another proxy used to investigate the rate of calcite precipitation and water availability. Growth rates calculated along the central growth axis are more robust than those calculated farther away and closer to the flanks. This is because growth layers tend to thin and pinch further away from the central growth axis and the probability of over- or underestimating growth rate is heightened. However, there are many times where speleothem samples with complex internal morphologies are the only samples available for paleoclimate research.

Various studies have been performed for identifying and prioritizing suitable speleothems (from a collection of candidates) for extracting specific kinds of paleoclimate data. Frappier (2008) provides a stepwise screening strategy to select stalagmites that may be sensitive to individual storms and thus may preserve a record of such events. Another study used a portable, energy-dispersive X-ray fluorescence probe as a fast and non-destructive in situ trace-element screener of speleothems to provide mineralogical information (Perrin et al., 2019). Recent studies from caves in Thailand have used XRCT specifically to discern the suitability of uncut speleothems as records of paleoclimate data based on assessing the internal growth history (Chawchai et al., 2018; Chawchai et al., 2020). Here, we build on these studies by incorporating the use of XRCT as a non-invasive and sustainable way of identifying and mapping simple, as well as complex, speleothem samples.

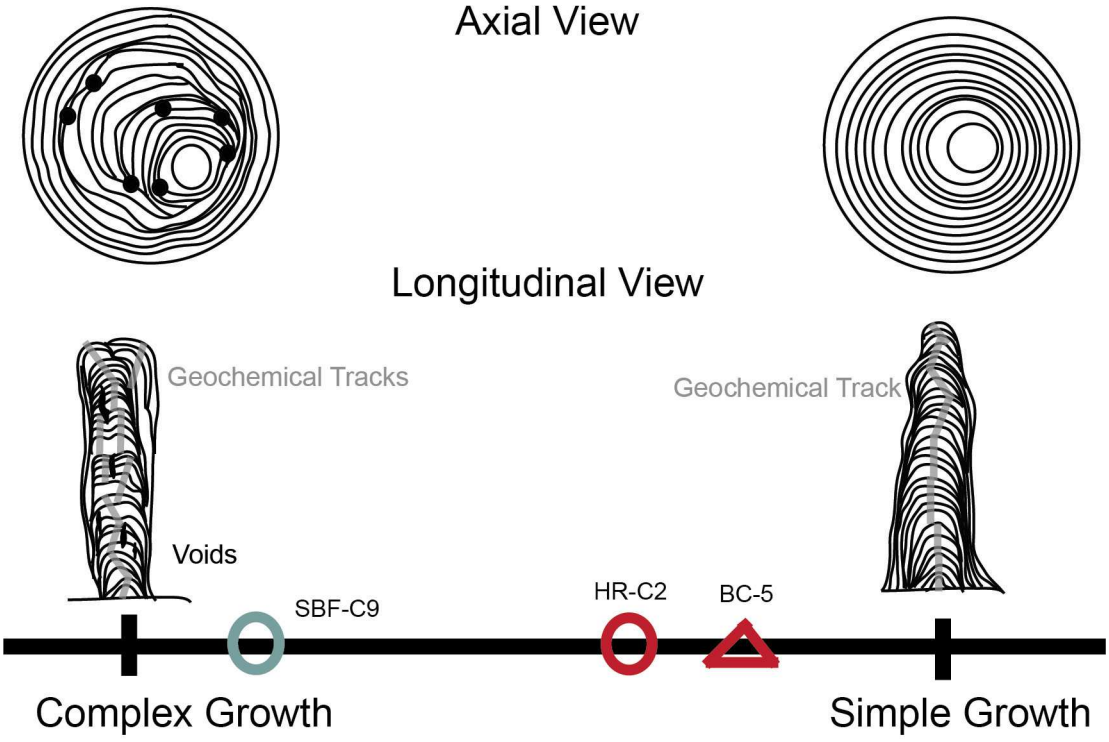

Figure 8. Suitability of stalagmite samples for paleoclimate reconstructions based on XRCT scans. Rapid, non-destructive, and relatively inexpensive XRCT scan imagery allows for constructing the growth history of stalagmite samples before destructive sampling. XRCT scans can reconstruct in detail the position and orientation of the growth axis for complex and simple speleothem morphologies over time. The non-destructively retrieved growth history can be used to (1) include more samples as candidates for paleoclimate analysis, (2) determine where they sit on the suitability spectrum, and (3) investigate proxies of shifting growth axis over time to capture changing paleoenvironment conditions. HRC2 and BC5 lie closer to the simple speleothem morphology. SBFC9 lies closer to the complex speleothem morphology. However, careful tracking of growth history of SBFC9 through XRCT scan imagery, we discern optimal locations for geochemical analyses that follows the migration of the growth axis. By demonstrating the utility of XRCT to track the complex internal morphology of an uncut sample, we increase the possibility of using such samples for paleoclimate reconstructions. Nonetheless, the task to retrieve a time-continuous paleoclimate record from the Complex Growth suitability section is relatively low.

By closely analyzing the axial and longitudinal XRCT views of the three speleothem samples (BC5, HRC2, and SBFC9), we reconstructed the history of migration of growth. SBFC9 growth displays significant lateral displacements, whereas in the other two samples, the lateral displacement is minimal. In addition to reconstructing the migration of growth, XRCT scans help characterize and identify internal morphological structures. These include growth

sections with (1) symmetrical and continuous growth along a singular apex of calcite precipitation, (2) uniform crystal morphology with a low number of hiatus features, and (3) spatial distribution of voids (Fig. 8).

In addition to internal growth structures, there are several other criteria that may influence speleothem sample selection. These include (1) inferred depositional processes such as hydrologic flow pathways (diffuse versus conduit flow feeding the stalagmite), (2) whether the speleothem is actively precipitating calcite, (3) calcite versus aragonite mineralogy of growth layers, (4) active cave flooding, and (5) cave ventilation regime. Briefly, hydrologic flow pathways, i.e., diffuse and conduit feeding drips, impact the amount of calcite precipitation and thereby the temporal resolution of the paleoclimate signal encapsulated in growth layers. Cave ventilation regimes can provide information on seasonal biases in calcite precipitation (James et al., 2015; Khazmutdinova et al., 2019). Cave ventilation and hydrological flow pathways can be discerned through continual monitoring of the cave environment. Active cave flooding further impacts the utility of speleothems as recorders of paleo-hydrology (Feinberg et al., 2020). Further, active calcite precipitation provides an age anchor for reconstructing the chronology and performing modern calcite growth experiments (Tremaine et al., 2011).

Based on the internal morphological characteristics identified above, we present a conceptual screening method that can be used by speleothem researchers to optimize paleoclimate reconstructions. We use two end-members as complex and simple stalagmite growth (Fig. 8). Simple endmember characteristics include (1) symmetrical growth along a singular apex of calcite precipitation with consistent growth layers, (2) continuous growth, (3) high-density calcite, and (4) minimum voids and hiatuses. Conversely, complex end-member characteristics include (1) multiple growth apices with complex growth sections, (2) an absence of consistent growth layers, (3) growth layers that are crosscutting and laterally noncontinuous, and (4) multiple voids and hiatuses.

Historically, samples that follow simple end-member characteristics have been easier to work with because geochemical sampling tracks are a single line drawn perpendicular to the growth axis (Fig. 8, gray lines). Such samples are ideal to reconstruct a temporally-continuous paleoclimate record. However, the simple end-member sample is not always available. For example, in SBF Cave most of the stalagmites have been vandalized; the cave is only left with samples that have complex internal morphologies. XRCT scans in such cases can optimize characterization of the internal growth history before slabbing stalagmites that are architecturally not simple but may be able to provide longer and continuous paleoclimate records from a climate-sensitive region that has a scarcity in stalagmite records.

As such, the utility of XRCT scans is expanded in this study by incorporating typically understudied complex stalagmites. Despite the complexities of SBFC9, XRCT scans helped locate the optimal slabbing planes for geochemical analyses. Nonetheless, determining transverse tracks (for radiometric dating) and perpendicular tracks (for stable isotope ratios and trace element concentrations) to retrieve hydroclimate data in such samples remains a challenge that requires additional scientific attention.

CONCLUSIONS

We build on the application of XRCT in speleothem science by reconstructing and comparing the growth histories of uncut stalagmites with both simple and complex internal morphologies. There are many occasions where speleothem scientists have access to a limited number of potential stalagmite samples for paleoclimate reconstructions. In such cases, using XRCT to appraise the internal morphology is crucial if the end goal is to retrieve a paleoclimate record. In this study, we show that careful investigation of XRCT scans can track the position and orientation of the growth sections of stalagmite samples that have complex morphologies. We demonstrate that XRCT scans capture the center of growth of stalagmites with simple internal morphologies by tracking the migration of concentric rings. Further, XRCT scans track the rims of micro-terraces as a cluster of low opacity points surrounding high opacity sections as calcite depositing basins in an uncut stalagmite sample. As such, samples that are low on the proposed suitability spectrum do not necessarily equate to unsuitable samples for paleoclimate reconstructions. XRCT scans can, in fact, be a guide in providing usable, albeit more complicated, sample transects along the center of growth. The information gained using XRCT further helps strategize the optimum plane(s) to perform the destructive and irreversible procedure of sectioning prior to geochemical analyses or retrieval of powders for radiometric dating. Additionally, if an uncut speleothem sample is deemed unsuitable for scientific purposes through XRCT scanning prior to destructively slabbing, it can easily be placed back in the cave.

For stalagmite SBFC9 from New Mexico, XRCT scans and PL images of the same slabbed face are used to locate growth layers for preliminary U-series dating. The criteria of subsampling sites with low porosity, visible and laterally continual growth layers, and minimum voids achieved through comparing XRCT scans with PL images provided adequate U and Th concentrations. Similarly, for stalagmite BC5 from Florida, XRCT scans and preliminary ^{14}C ages show that a thick layer of calcite overgrowth had precipitated down the flank on one side and resulted in miscalculation of targeted reconnaissance ages. Lastly, 3-dimensional visualization through XRCT scans of HRC2 from Florida highlights the presence of multiple voids. The voids are not present in the PL images, and the 3-dimensional visualization

suggests that voids persist deeper than just the surface. Therefore, comparison between PL images and XRCT scans can be a guide in avoiding voids, which impact geochemical analyses through detrital contamination and the presence of diagenetically altered calcite.

ACKNOWLEDGEMENTS

The authors would like to thank Drs. Matthew Colbert and Jessica Maisano with assistance in XRCT scanning of SBFC9 at the High-Resolution X-Ray Computed Tomography Facility at The University of Texas at Austin, and Don McCardle for scanning HRC2 and BC5 at Capital Regional Medical Center in Tallahassee, Florida. Dr. Nate Miller analyzed samples on the quadrupole inductively-coupled plasma mass spectrometer at the University of Texas at Austin for U and Th concentrations. The authors would also like to thank Aaron Stockton, Lincoln National Forest Service Cave Manager, for allowing us a permit, facilitating research, and providing key logistical support to core the sample from Sitting Bull Falls Cave, as well as Allen Mosler, Leon Brooks, and the Southeastern Cave Conservancy Inc. for access to HRC2 and BC5. We thank Harley Means and Bruce Means for their unwavering resolve to rescue BC5 from a partially collapsed cave. Financial support for the work done is from the Geological Science Association graduate student grant awarded to N. Sekhon. N. Sekhon was supported by NSF Grant AGS-1912100 to Drs. C. Wong and D. Breecker. D. Tremaine was supported by NSF Grant AGS-1032403 to P.N. Froelich, the Department of Oceanography, and the National High Magnetic Field Laboratory, Florida State University. Dr. Banner would like to thank funding from NSF P2C2 grant, #AGS-2203052 for support. The authors would also like to acknowledge funding from the University of Texas at Austin, Planet Texas 2050 PaleoTexas grant.

REFERENCES

Abràmoff, M.D., Magalhães, P.J., and Ram, S.J., 2004, Image processing with ImageJ: Biophotonics International, v. 11, p. 36–42, https://imagej.nih.gov/ij/docs/pdfs/Image_Processing_with_ImageJ.pdf.

Atsawawaranunt, K., et al., 2018, The SISAL database: A global resource to document oxygen and carbon isotope records from speleothems: Earth System Science Data, v. 10, p. 1687–1713, https://doi.org/10.5194/essd-10-1687-2018.

Bajo, P., et al., "Cryptic" diagenesis and its implications for speleothem geochronologies: Quaternary Science Reviews, v. 148, p. 17–28, https://doi.org/10.1016/j.quascirev.2016.06.020.

Baldini, J.U.L., 2001, Morphologic and dimensional linkage between recently deposited speleothems and drip water from Browns Folly Mine, Wiltshire, England: Journal of Cave and Karst Studies, v. 63, p. 83–90, https://caves.org/wp-content/uploads/2022/05/cave_63-03-fullr.pdf.

Banner, J.L., Guilfoyle, A., James, E.W., Stern, L.A., and Musgrove, M., 2007, Seasonal variations in modern speleothem calcite growth in central Texas, U.S.A.: Journal of Sedimentary Research, v. 77, p. 615–622, https://doi.org/10.2110/jsr.2007.065.

Boch, R., Spötl, C., and Frisia, S., 2011, Origin and palaeoenvironmental significance of lamination in stalagmites from Katerloch Cave, Austria: Sedimentology, v. 58, p. 508–531, https://doi.org/10.1111/j.1365-3091.2010.01173.x.

Carlson, W.D., Rowe, T., Ketcham, R.A., and Colbert, M.W., 2003, Applications of high-resolution X-ray computed tomography in petrology, meteoritics and palaeontology: Geological Society, London, Special Publications, v. 215, p. 7–22, https://doi.org/10.1144/GSL.SP.2003.215.01.02.

Carlson, P.E., Noronha, A.L., Banner, J.L., Jenson, J.W., Moore, M.W., Partin, J.W., Deininger, M., Breecker, D.O., and Bautista, K.K., 2020, Constraining speleothem oxygen isotope disequilibrium driven by rapid CO_2 degassing and calcite precipitation: Insights from monitoring and modeling: Geochimica et Cosmochimica Acta, v. 284, p. 222–238, https://doi.org/10.1016/j.gca.2020.06.012.

Chawchai, S., Liu, G., Bissen, R., Jankham, K., Paisonjumlongsri, W., Kanjanapayont, P., Chutakositkanon, V., Choowong, M., Pailoplee, S., and Wang, X., 2018, Stalagmites from western Thailand: Preliminary investigations and challenges for palaeoenvironmental research: Boreas, v. 47, p. 367–376, https://doi.org/10.1111/bor.12299.

Chawchai, S., Liu, G., Bissen, R., Scholz, D., Riechelmann, D.F.C., Vonhof, H., Mertz-Kraus, R., Chiang, H.-W., Tan, L., and Wang, X., 2020, Hydroclimate variability of western Thailand during the last 1400 years: Quaternary Science Reviews, v. 241, p. 106423,
https://doi.org/10.1016/j.quascirev.2020.106423.

Cnudde, V., and Boone, M.N., 2013, High-resolution X-ray computed tomography in geosciences: A review of the current technology and applications: Earth-Science Reviews, v. 123, p. 1–17, https://doi.org/10.1016/j.earscirev.2013.04.003.

Comas-Bru, L., et al., 2020, SISALv2: A comprehensive speleothem isotope database with multiple age-depth models: Earth System Science Data, v. 12, p. 2579–2606, https://doi.org/10.5194/essd-12-2579-2020.

Czuppon, G., Demény, A., Leél-Őssy, S., Óvari, M., Molnár, M., Stieber, J., Kiss, K., Kármán, K., Surányi, G., and Haszpra, L., 2018, Cave monitoring in the Béke and Baradla Caves (Northeastern Hungary): Implications for the conditions for the formation cave carbonates: International Journal of Speleology, v. 47, p. 13–28, https://doi.org/10.5038/1827-806X.47.1.2110.

Dreybrodt, W., 1999, Chemical kinetics, speleothem growth and climate: Boreas, v. 28, p. 347–356, https://doi.org/10.1111/j.1502-3885.1999.tb00224.x.

Dreybrodt, W., and Gabrovšek, F., 2009, Small-scale terraces and isolated rimstone pools on stalagmites in caves exhibit striking similarity to large-scale terrace landscapes at hot springs: Acta Carsologica, v. 38, p. 19–26, https://doi.org/10.3986/ac.v38i1.133.

Dreybrodt, W., Hansen, M., and Scholz, D., 2016, Processes affecting the stable isotope composition of calcite during precipitation on the surface of stalagmites: Laboratory experiments investigating the isotope exchange between DIC in the solution layer on top of a speleothem and the CO_2 of the cave atmosphere: Geochimica et Cosmochimica Acta, v. 174, p. 247–262, https://doi.org/10.1016/j.gca.2015.11.012.

Du Preez, G., du Plessis, A., de Beer, D., and Forti, P., 2018, Non-destructive, high-resolution X-ray micro-CT of a hairy stalagmite: investigating the structural details of a biogenic speleothem: International Journal of Environmental Science and Technology, v. 15, p. 1843–1850, https://doi.org/10.1007/s13762-017-1543-4.

Fairchild, I.J., and Baker, A., 2012, Speleothem Science: From Process to Past Environments: Oxford, Wiley-Blackwell, 432 p., https://doi.org/10.1002/9781444361094.

Fairchild, I.J., and Treble, P.C., 2009, Trace elements in speleothems as recorders of environmental change: Quaternary Science Reviews, v. 28, p. 449–468, https://doi.org/10.1016/j.quascirev.2008.11.007.

Feinberg, J.M., Lascu, I., Lima, E.A., Weiss, B.P., Dorale, J.A., Alexander, E.C., Jr., and Edwards, R.L., 2020, Magnetic detection of paleoflood layers in stalagmites and implications for historical land use changes: Earth and Planetary Science Letters, v. 530, p. 115946, https://doi.org/10.1016/j.epsl.2019.115946.

Frappier, A.B., 2008, A stepwise screening system to select storm-sensitive stalagmites: Taking a targeted approach to speleothem sampling methodology: Quaternary International, v. 187, p. 25–39, https://doi.org/10.1016/j.quaint.2007.09.042.

Frisia S., 2015, Microstratigraphic logging of calcite fabrics in speleothems as tool for palaeoclimate studies: International Journal of Speleology, v. 44, p. 1–16, https://doi.org/10.5038/1827-806X.44.1.1.

Froelich, P.N., Kowalczk, A.J., McCardle, D., and Tibbetts, N., 2007, Speleothem paleoclimate records from the Floridian Panhandle: Abstract PP43A-0998, presented at 2007 Fall Meeting, American Geophysical Union, San Francisco, 10–14 December.

Hammer, Ø., Dysthe, D.K., and Jamtveit, B., 2007, The dynamics of travertine dams: Earth and Planetary Science Letters, v. 256, p. 258–263, https://doi.org/10.1016/j.epsl.2007.01.033.

Hammer, Ø., Dysthe, D.K., and Jamtveit, B., 2010, Travertine terracing: Patterns and mechanisms: Geological Society, London, Special Publications, v. 336, p. 345–355, https://doi.org/10.1144/SP336.18.

Hayes, P.T., 1964, Geology of the Guadalupe Mountains, New Mexico, Geological Survey Professional Paper 446, Washington: US Government Printing Office, 68 p., https://doi.org/10.3133/pp446.

Hill, C.A., 2000, Overview of the geologic history of cave development in the Guadalupe Mountains, New Mexico: Journal of Cave and Karst Studies, v. 62, p. 60–71, https://caves.org/wp-content/uploads/2022/05/cave_62-02-fullr.pdf.

James, E.W., Banner, J.L., and Hardt, B., 2015, A global model for cave ventilation and seasonal bias in speleothem paleoclimate records: Geochemistry, Geophysics, Geosystems, v. 16, p. 1044–1051, https://doi.org/10.1002/2014GC005658.

Jettestuen, E., Jamtveit, B., Podladchikov, Y.Y., deVilliers, S., Amundsen, H.E.F., and Meakin, P., 2006, Growth and characterization of complex mineral surfaces, Earth and Planetary Science Letters, v. 249, p. 108–118, https://doi.org/10.1016/j.epsl.2006.06.045.

Kaufmann, G., and Dreybrodt, W., 2004, Stalagmite growth and palaeo-climate: An inverse approach: Earth and Planetary Science Letters, v. 224, p. 529–545, https://doi.org/10.1016/j.epsl.2004.05.020.

Ketcham, R.A. and Carlson, W.D., 2001, Acquisition, optimization and interpretation of X-ray computed tomographic imagery: Applications to the geosciences: Computers and Geosciences, v. 27, p. 381–400, https://doi.org/10.1016/S0098-3004(00)00116-3.

Khazmutdinova, K., Nof, D., Tremaine, D.M., Ye, M., and Moore, M.N.J., 2019, A minimal model for predicting ventilation rates of subterranean caves, Journal of Cave and Karst Studies, vol. 81, p. 264–275, https://doi.org/10.4311/2018ES0141.

Kowalczk, A., 2009, High resolution microclimate study of Hollow Ridge Cave: Relationships between cave meteorology, air chemistry, and hydrology and the impact on speleothem deposition [M.S. thesis], Florida State University, 238 p., http://purl.flvc.org/fsu/fd/FSU_migr_etd-2853.

Lachniet, M.S., 2009, Climatic and environmental controls on speleothem oxygen-isotope values: Quaternary Science Reviews, v. 28, p. 412–432, doi.org/10.1016/j.quascirev.2008.10.021.

Martín-Chivelet, J., Muñoz-García, M.B., Cruz, J.A., Ortega, A.I., and Turrero, M.J., 2017, Speleothem architectural analysis: Integrated approach for stalagmite-based paleoclimate research: Sedimentary Geology, v. 353, p. 28–45, https://doi.org/10.1016/j.sedgeo.2017.03.003.

McDermott, F., 2004, Palaeo-climate reconstruction from stable isotope variations in speleothems: A review: Quaternary Science Reviews, v. 23, p. 901–918, https://doi.org/10.1016/j.quascirev.2003.06.021.

Mickler, P.J., Stern, L.A., and Banner, J.L., 2006, Large kinetic isotope effects in modern speleothems: Geological Society of America Bulletin, v. 118, p. 65–81, https://doi.org/10.1130/B25698.1.

Mickler, P.J., Ketcham, R.A., Colbert, M.W., and Banner, J.L., 2004, Application of high-resolution X-ray computed tomography in determining the suitability of speleothems for use in paleoclimatic, paleohydrologic reconstructions: Journal of Cave and Karst Studies, v. 66, p. 4–8, https://caves.org/wp-content/uploads/2022/05/cave_66-01-fullr.pdf.

Miller, A.Z., De la Rosa, J., Jiménez-Morillo, N.T., Pereira, M.F.C., Gonzalez-Perez, J.A., Knicker, H., and Saiz-Jimenez, C., 2020, Impact of wildfires on subsurface volcanic environments: New insights into speleothem chemistry: Science of the Total Environment, v. 698, p. 134321, https://doi.org/10.1016/j.scitotenv.2019.134321.

Muñoz-García, M.B., Cruz, J., Martín-Chivelet, J., Ortega, A.I., Turrero, M.J., and López-Elorza, M., 2016, Comparison of speleothem fabrics and microstratigraphic stacking patterns in calcite stalagmites as indicators of paleoenvironmental change: Quaternary International, v. 407, p. 74–85, https://doi.org/10.1016/j.quaint.2016.02.036.

Nymeyer, R., 1978, Carlsbad, Caves, and a Camera: Teaneck, N.J., Zephyrus Press, 328 p.

Perrin, C., Tilhac, R., and Prestimonaco, L., 2019, Optimizing subsampling strategies for U/Th dating and geochemical proxies in carbonate speleothems: Sedimentary Geology, v. 389, p. 91–102, https://doi.org/10.1016/j.sedgeo.2019.06.002.

Romanov, D., Kaufmann, G., and Dreybrodt, W., 2008, Modeling stalagmite growth by first principles of chemistry and physics of calcite precipitation: Geochimica et Cosmochimica Acta, v. 72, p. 423–437, https://doi.org/10.1016/j.gca.2007.09.038.

Scroxton, N., et al., 2016, Natural attrition and growth frequency variations of stalagmites in southwest Sulawesi over the past 530,000 years: Palaeogeography, Palaeoclimatology, Palaeoecology, v. 441, p. 823–833, https://doi.org/10.1016/j.palaeo.2015.10.030.

Sekhon, N., Banner, J.L., Black, B., Miller, N., and Breecker, D.O., 2019, High-resolution stalagmite record examining local hydroclimate variability from a shallow cave in semi-arid New Mexico: Geological Society of America Abstracts with Programs, v. 51 no. 5, paper no. 89-12, https://doi.org/10.1130/abs/2019AM-339286.

Shtober-Zisu, N., Schwarcz, H.P., Chow, T., Omelon, C.R., and Southam, G., 2014, Caves in caves: Evolution of post-depositional macroholes in stalagmites: International Journal of Speleology, v. 43, p. 323–334, https://doi.org/10.5038/1827-806X.43.3.9.

Spötl, C., and Mattey, D., 2012, Scientific drilling of speleothems—a technical note: International Journal of Speleology, v. 41, p. 4, https://doi.org/10.5038/1827-806X.41.1.4.

Spötl, C., Fairchild, I.J., and Tooth, A.F., 2005, Cave air control on dripwater geochemistry, Obir Caves (Austria): Implications for speleothem deposition in dynamically ventilated caves: Geochimica et Cosmochimica Acta, v. 69, p. 2451–2468, https://doi.org/10.1016/j.gca.2004.12.009.

Tremaine, D.M., 2010, Speleothem paleoclimatology and modern speleochemistry proxies: Calcite farming in a continuously monitored cave [M.S. thesis], Florida State University, 227 p., http://purl.flvc.org/fsu/fd/FSU_migr_etd-1523.

Tremaine, D.M., 2015, Dynamic physicochemical influences on speleothem paleoclimate proxy archives: A story of four north Florida caves [Ph.D. dissertation]: Florida State University, 267 p., http://purl.flvc.org/fsu/fd/FSU_migr_etd-9473.

Tremaine, D.M., Froelich, P.N., and Wang, Y., 2011, Speleothem calcite farmed in situ: Modern calibration of $\delta^{18}O$ and $\delta^{13}C$ paleoclimate proxies in a continuously-monitored natural cave system: Geochimica et Cosmochimica Acta, v. 75, p. 4929–4950, https://doi.org/10.1016/j.gca.2011.06.005.

Tremaine, D.M., Sinclair, D.J., Stoll, H.M., Lagerström, M., Carvajal, C.P., and Sherrell, R.M., 2016, A two-year automated dripwater chemistry study in a remote cave in the tropical south Pacific: Using [Cl^-] as a conservative tracer for seasalt contribution of major cations: Geochimica et Cosmochimica Acta, v. 184, p. 289–310, https://doi.org/10.1016/j.gca.2016.03.029.

Vanghi, V., Iriarte, E., and Aranburu, A., 2015, High resolution X-ray computed tomography for petrological characterization of speleothems: Journal of Cave and Karst Studies, v. 77, p. 75–82, https://doi.org/10.4311/2014ES0102.

Van Breukelen, M.R., Vonhof, H.B., Hellstrom, J.C., Wester, W.C.G., and Kroon, D., 2008, Fossil dripwater in stalagmites reveals Holocene temperature and rainfall variation in Amazonia: Earth and Planetary Science Letters, v. 275, p. 54–60, https://doi.org/10.1016/j.epsl.2008.07.060.

Walczak, I.W., Baldini, J.U.L., Baldini, L.M., McDermott, F., Marsden, S., Standish, C.D., Richards, D.A., Andreo, B., and Slater, J., 2015, Reconstructing high-resolution climate using CT scanning of unsectioned stalagmites: A case study identifying the mid-Holocene onset of the Mediterranean climate in southern Iberia: Quaternary Science Reviews, v. 127, p. 117–128, https://doi.org/10.1016/j.quascirev.2015.06.013.

Webster, J.W., Brook, G.A., Railsback, L.B., Cheng, H., Edwards, R.L., Alexander, C., and Reeder, P.P., 2007, Stalagmite evidence from Belize indicating significant droughts at the time of Preclassic Abandonment, the Maya Hiatus, and the Classic Maya collapse: Palaeogeography, Palaeoclimatology, Palaeoecology, v. 250, p. 1–17, https://doi.org/10.1016/j.palaeo.2007.02.022.

Wortham, B.E., Montañez, I.P., Rowland, D.J., Lerche, M., and Browning, A., 2019, Mapping fluid□filled inclusions in stalagmites using coupled x-ray and neutron computed tomography: Potential as a water excess proxy: Geochemistry, Geophysics, Geosystems, v. 20, p. 2647–2656, https://doi.org/10.1029/2018GC008140.

Wong, C.I. and Breecker, D.O., 2015, Advancements in the use of speleothems as climate archives: Quaternary Science Reviews, v. 127, p. 1–18, https://doi.org/10.1016/j.quascirev.2015.07.019.

Wong, C.I., Banner, J.L., and Musgrove, M., 2011, Seasonal dripwater Mg/Ca and Sr/Ca variations driven by cave ventilation: Implications for and modeling of speleothem paleoclimate records: Geochimica et Cosmochimica Acta 75, p. 3514–3529, https://doi.org/10.1016/j.gca.2011.03.025.

Zisu, N.S., Schwarcz, H.P., Konyer, N., Chow, T., and Noseworthy, M.D., 2012, Macroholes in stalagmites and the search for lost water: Journal of Geophysical Research: Earth Surface, v. 117, 14 p., https://doi.org/10.1029/2011JF002288.

SUPPLEMENTARY FILES

Animations for the 3 analyzed speleothems (HRC2, BC5, and SBFC9) are found at https://github.com/nsekhon91/XRCT_Animations. The folder contains 3 XRCT scans in the respective speleothems axial planes:

Stalagmite from Hollow Ridge Cave, Florida: HRC2 Axial Animation.mov

Stalagmite from Brooks Quarry Cave, Florida: BC5 Axial Animation.mov

Stalagmite from SBF Cave, New Mexico: SBFC9 Axial Animation.mov

To view the animations, the reader has to download the files.